NeuroImage: Clinical 35 (2022) 103062

Contents lists available at ScienceDirect

NeuroImage: Clinical

journal homepage: www.elsevier.com/locate/ynicl

Differential tractography as a dynamic imaging biomarker: A methodological pilot study for Huntington's disease

Jessica V. Barrios-Martinez [a,1], David T. Fernandes-Cabral [a,1], Kumar Abhinav [e], Juan C. Fernandez-Miranda [d], Yue-Fang Chang [a,b], Valerie Suski [c], Fang-Cheng Yeh [a,b,*], Robert M. Friedlander [a,*]

[a] Department of Neurological Surgery, University of Pittsburgh, UPMC, Pittsburgh, PA, USA
[b] Department of Bioengineering, University of Pittsburgh, Pittsburgh, PA, USA
[c] Department of Neurology, University of Pittsburgh, UPMC, Pittsburgh, PA, USA
[d] Department of Neurological Surgery, Stanford University, Stanford, CA, USA
[e] Department of Neurosurgery, University of Bristol, Southmead Hospital, Bristol, UK

ARTICLE INFO

Keywords:
Huntington's disease
Differential tractography
UHDRS
Diffusion MRI
Biomarker

ABSTRACT

Huntington's disease (HD) is a neurodegenerative disorder characterized by motor, psychiatric, and cognitive symptoms. Due to its diverse manifestations, the scientific community has long recognized the need for sensitive, objective, individualized, and dynamic disease assessment tools. We examined the feasibility of Differential Tractography as a biomarker to evaluate correlation of symptom severity and of HD progression at the individual level. Differential tractography is a novel tractography modality that maps pathways with axonal injury characterized by a decrease of anisotropic diffusion pattern. We recruited sixteen patients scanned at 0-, 6-, and 12-month intervals by diffusion MRI scans for differential tractography assessment and correlated its volumetric findings with the Unified Huntington's Disease Rating Scale (UHDRS). Deterministic fiber tracking algorithm was applied. Longitudinal data was modeled using the generalized estimating equation (GEE) model and correlated with UHDRS scores, in addition to Spearman correlation for cross-sectional data. Our results show that volumes of affected pathways revealed by differential tractography significantly correlated with UHDRS scores in longitudinal data (p-*value* < 0.001), and chronological changes in differential tractography also correlated with the changes in UHDRS (p-*value* < 0.001). This technique opens new clinical avenues as a clinical translational tool to evaluate presymptomatic and symptomatic gene positive individuals. Our results provide support that differential tractography has the potential to be used as a dynamic imaging biomarker to assess at the individual level in a non-invasive manner, disease progression in HD. Critically important, differential tractography proves to be a quantitative tool for following degeneration in presymptomatic patients, with potential applications in clinical trials.

1. Introduction

Huntington's disease (HD) is a progressive chronic neurodegenerative disorder, resulting from a mutation in the huntingtin gene consisting of a CAG repeat expansion. The resulting protein has an expanded glutamine repeat near the N-terminus, resulting in a toxic gain of function. No effective treatment is available for HD, and the disease is universally fatal. Hallmarks of HD include choreic movements, extrapyramidal motor abnormalities, and cognitive impairment. HD patients may also present with behavioral abnormalities including anxiety, depression and compulsive behaviors (Craufurd et al., 2001). A reliable approach to evaluate disease severity and progression has been challenging in HD. The assessment of the severity of clinical symptoms relies mostly on the Unified Huntington's Disease Rating Scale (UHDRS) for disease stage stratification (Kieburtz et al., 2001). UHDRS evaluates the motor, cognitive, behavioral, and functional capacity allowing for a quantitative assessment based on clinical presentation. Despite the usefulness of UHDRS, there is still an ongoing need for an objective

* Corresponding authors at: Department of Neurological Surgery, University of Pittsburgh, Pittsburgh, Pennsylvania, USA (F.-C. Yeh).
E-mail addresses: frank.yeh@pitt.edu (F.-C. Yeh), friedlanderr@upmc.edu (R.M. Friedlander).
[1] Co-First Author.

https://doi.org/10.1016/j.nicl.2022.103062
Received 25 March 2022; Received in revised form 5 May 2022; Accepted 26 May 2022
Available online 28 May 2022

imaging biomarker to assess disease onset, progression, and severity.

Studies such as PREDICT-HD (Biglan et al., 2009) and TRACK-HD (Tabrizi et al., 2009) have used standard MRI to quantify gross structural findings and investigate the correlation between neuroimaging findings with cognitive and biological imaging and motor outcome measures. TRACK-HD correlated volumetric MRI with UHDRS in premanifest and manifest patients. Both PREDICT-HD and TRACK-HD confirmed previous reports supporting the value of imaging markers, especially of striatal and whole-brain atrophy during the premanifest stage (Biglan et al., 2009; Tabrizi et al., 2009). A recent study (Zeun et al., 2022) that applied fixel-based analysis in a large sample of premanifest individuals suggests that white matter structures such as the cortico-basal ganglia display signs of degeneration or *"vulnerability"* at around 11–25 years after diagnosis, with preserved integrity as early as 25 years before diagnosis has been established. In addition, the aforementioned study observed that the sensory and motor components of the thalamus and the limbic and motor striatum have demonstrated to be at risk in this population, suggesting that clear observable white matter changes at the voxel level can be demonstrated years after diagnosis and not during the premanifest phase. These interesting findings allow the opportunity for the emergence of biomarkers capable of detecting onset of neurodegeneration before clinical manifestations, which in turn, with early initiation of disease modifying therapies, can potentially represent a better quality of life for these patients. Other studies have shown that white matter atrophy is evident in T1-weighted MRI with posterior-frontal white matter degeneration evident in at-risk individuals far from disease onset (Tabrizi et al., 2009). Structural MRI allows for the examination of gradual changes that occur in premanifest HD with MRI studies showing that these subjects have brain atrophy years before disease manifestation in pyramidal projection neurons in the motor and prefrontal cortices, and cingulate and angular gyri (Macdonald and Halliday, 2002; Thu et al., 2010). However, volumetric findings in the above-mentioned studies applied a group-based approach and individual difference are of the utmost importance for clinical applications. Although it is recognized that structural MRI has been sensitive to measure for neuronal loss and total volume measurement in grey and white matter cortical areas (Tan et al., 2021), there is still ongoing efforts to increase the search for specific markers for localization of volume loss and atrophy (Adanyeguh et al., 2021).

White matter changes have been studied by implementing diffusion MRI to explore its clinical value in neurodegeneration. Techniques such as Diffusion Tensor Imaging (DTI) (Basser et al., 1994) are capable of detecting structural changes in axonal pathways in HD patients (Dumas et al., 2012; Georgiou-Karistianis et al., 2011; Gregory et al., 2015; Klöppel et al., 2008; Phillips et al., 2013; Poudel et al., 2014; Rosas et al., 2010; Ross et al., 2014; Weaver et al., 2009). Disruption of several white matter pathways including cortico-striatal motor projections, cingulum, uncinate fasciculus, thalamocortical projections, corpus callosum, and corticospinal tract, have been found in HD (Dumas et al., 2012; Georgiou-Karistianis et al., 2011; Müller et al., 2013; Nopoulos et al., 2010; Phillips et al., 2013; Rosas et al., 2010; Weaver et al., 2009). Furthermore, cognitive and motor parameters correlated with white matter DTI alterations in several studies (Dumas et al., 2012; Georgiou-Karistianis et al., 2011; Gregory et al., 2015; Phillips et al., 2013; Poudel et al., 2014; Rosas et al., 2010; Ross et al., 2014; Weaver et al., 2009). DTI remains a commonly used technique to study structural white matter changes in neurodegeneration, however, its clinical applications are limited due to its inability to resolve complex fiber orientations in the presence of free water (i.e. CSF volume acting as an artifact) (Berlot et al., 2014; Jeurissen et al., 2013; Metzler-Baddeley et al., 2012), while still only demonstrating a difference in HD patients at a group level when compared to a control population. Recent studies have applied beyond-DTI methods such as fixel-based analyses using constraint spherical deconvolution (CSD) in early HD (Adanyeguh et al., 2021; Oh et al., 2021) and in premanifest HD (Zeun et al., 2022) to identify neurodegeneration in HD. However, although the fixel-based approach provides a high angular resolution advantage (Tournier et al., 2004), several technical considerations need to be taken to avoid a critical flaw in tractography clinical studies (Parker et al., 2013). Furthermore, the acceptance that DTI-based metrics are non-specific for neurodegeneration and disease progression assessment, warrants the opportunity to move beyond DTI-based approaches (Farquharson et al., 2013; Fernandez-Miranda, 2013; Tournier et al., 2004).

Recently advanced diffusion MRI has acquired a more sophisticated diffusion model by resolving multiple diffusion sensitization and hundreds of diffusion sampling directions (Sotiropoulos et al., 2013). This significant improvement has allowed to resolve complex fiber orientation by using or resorting to a nonparametric approach (Tuch et al., 2003). This has led to the development of beyond-DTI tractography that can handle crossing-fibers (Tournier et al., 2011) and cope with the partial volume of free water (Zhang et al., 2013). Beyond-DTI tractography has been used in patients with aphasia to demonstrate a clear functional correlation of tractography white matter fiber bundles such as the arcuate fasciculus (AF), inferior longitudinal fasciculus (IFOF), uncinate fasciculus (UF), and middle longitudinal fasciculus (MdLF) with semantic and phonological abilities involved in language production (Hula et al., 2020). Conventional tractography is not sensitive during early neuronal degeneration as tractography differences can only be demonstrated if anisotropy drops substantially below the tracking threshold, and although diffusion MRI has been explored as a potential biomarker for early onset neurodegeneration, anisotropy as a measurement at the voxel level is susceptible to local variability including but not limited to partial volume effect (Henf et al., 2018; Wang et al., 2011; Yeh et al., 2019) restricting its potential in the clinical setting (Melonakos et al., 2011; Yeh et al., 2019). Our recent study demonstrated that differential tractography (Yeh et al., 2019) addressed these limitations by focusing on differences in anisotropy to track only the segment of the pathway with neuronal degeneration. In the aforementioned study, the analysis required two longitudinal scans of the same subjects to derive differences, but in the present study we implemented an advanced protocol that compared one patient's scan with a cohort of control subjects. Differential tractography accomplishes a substantial improvement when compared to conventional tractography. The method performs a comparison of voxel-wise differences of diffusion properties, such as quantitative anisotropy (QA), allowing to only track changes resulting in highlighted tractograms with segments of degeneration. Volumes extracted from obtained tractograms result in a simple measurement of the amount of neurodegeneration. The volume of specific pathways with a decrease in anisotropy was used as a quantitative biomarker to correlate with clinical UHDRS scores. This novel modification allowed us to derive a numeric value of altered pathways for individual patients, hence enabling the opportunity to study the advantages of a true diffusion-based analysis technique as a clinical translational biomarker for early neuronal injury, in contrast to other technique such as Tractwise Fractional Anisotropy Statistics (TFAS) which applies fiber tracks as a skeleton to obtain underlying voxel Fractional Anisotropy (FA) for statistical analysis (Müller et al., 2016). Furthermore, since differential tractography tracks neuronal injury along a fiber pathway, this provides the ability to differentiate true findings from errors occurring at the local voxel level, as errors generated locally stay withing the local limits, versus true neuronal injury that disseminates along axons (Yeh et al., 2019).

In the present study we applied differential tractography in premanifest and manifest HD to localize differences in anisotropy between base and repeat scans, along with statistical correlation of anisotropic differences with UHDRS clinical scores, including total motor score (UHDRS TMS), dystonia total, chorea total, rapid alternating movements (RAM), stroop color word, behavior, and total functional capacity (UHDRS TFC). In addition, compromised fiber pathways in HD patients were identified by comparing them with healthy controls and quantifying the volume of each affected pathways as a biomarker. Although we have not taken in consideration any hypothesis to specific

white matter bundles, our study is exploratory, and we hypothesized that pathway alterations would correlate with the UHDRS in both cross-sectional and longitudinal settings. We demonstrate progressive degeneration as subjects were imaged at several time points and provide evidence that differential tractography can be used as a dynamic biomarker for progressive structural damage, which correlates with disease progression in HD patients.

2. Materials and methods

2.1. Patient characteristics and demographics

We recruited sixteen patients, including twelve manifest HD patients and four pre-manifest patients (Table 1). All patients gave their informed consent prior to their inclusion in the study. Manifest were symptomatic and pre-manifest were asymptomatic (all confirmed gene positive). Patients had three scans over a period of two years. Twelve patients had three scans, one patient had two scans, and three patients had one scan. The average scan interval from the first to the second scan was 6 ± 0.4 months (range 5 to 10 months) and the average scan interval from the first to the third scan was 12 ± 1 months (range 11 to 24 months). Patients underwent a comprehensive clinical evaluation on the day of the scan conducted by a neurologist specializing in movement disorders. Previous to each MRI, subjects were evaluated to assess their Unified Huntington Disease Rating Scale (UHDRS) (Kieburtz et al., 2001) scores, including motor, behavior, cognitive and functional assessments. A reconstructed averaged template was included from the CMU-60 database, a compiled diffusion MRI dataset of 60 healthy individuals acquired with a 257-diffusion sampling direction that served as control for our study.

2.2. MRI acquisition

Diffusion spectrum imaging data were acquired on a 3 T Tim Trio System (Siemens, Erlangen, Germany) using a 32-channel coil. A head stabilizer was utilized to prevent head motion. A 25 min, 257-direction DSI scan with a twice-refocused spin-echo planar imaging sequence and multiple *b* values (repetition time = 9916 ms, echo time = 157 ms, voxel size = 2.4 mm × 2.4 mm × 2.4 mm, field of view = 231 mm × 231 mm, maximum *b*-value = 7000 s/mm^2) was performed. For anatomical comparison, we included a high-resolution anatomical image using a 9-min T1-weighted axial MPRAGE sequence (repetition time = 2110 ms, echo time = 2.63 ms, flip angle = 8°, number of slices = 176, field of view = 256 mm × 256 mm, voxel size = 0.35 mm × 0.5 mm × 1.0 mm). We have used the same scanner as in the control population (CMU 60). The potential impact of the use of different scanners is addressed in the discussion section.

2.2.1. Differential tractography for individuals

The flowchart of our revised differential tractography (Yeh et al., 2013a) analysis is demonstrated in Fig. 1. Diffusion imaging data of each patient (Fig. 1A) was reconstructed to a common stereotaxic space using q-space diffeomorphic reconstruction (QSDR) (Yeh et al., 2010; Yeh and Tseng, 2011), which is a method that satisfies the conservation of diffusible spins and reconstructs diffusion MRI data in a common standard space. QSDR was applied to generate the density distribution of anisotropic diffusion (Fig. 1B). The red–greenblue colors represents the orientation of diffusion (red: left–right, green: anterior-posterior, blue: superior-inferior). QSDR allowed us to calculate the differences in anisotropic diffusion by comparing it with a normal population database (CMU-60 database, Fig. 1C) (Beukema et al., 2015; Donos et al., 2016) to show the locations of local fibers with a decrease of anisotropic diffusion in study subjects, indicating changes in fiber integrity. We used a percentile rank lower than 5 of the decrease in anisotropy as the threshold to filter the results. Fig. 1D shows the piecewise fibers (color-coded by orientation) with substantial decreases, which were connected to guide the fiber tracking algorithm to map the exact segment of affected fiber bundles (Fig. 1E). Fiber bundles were segmented based on a recent tractography atlas (Yeh et al., 2018) by using DSI Studio's interface for manual fiber tracking and we cross referenced with the average population atlas. The tracking was determined using a deterministic fiber-tracking algorithm (Yeh et al., 2013b) in our proprietary developed and open-source software DSI Studio (http://dsi-studio.labsolver.org). Deterministic tractography applies quantitative anisotropy (QA) which relies on generalized q-sampling imaging (GQI) to estimate the orientation of individual fibers (Yeh et al., 2010), and spin distribution function (SDF) to provide the amount or density of diffusing water in any direction within a single voxel (Yeh et al., 2016), therefore posing a great advantage over widely used diffusivity-based estimations such as FA. The tracking begins from each local fiber orientation as seeds and propagates until no orientation is found in the propagation direction. A maximum turning angle of 60° was used with a step size of 1 mm. The determined trajectories, termed the affected tracts, are used to identify pathways with decreased connectivity.

Table 1
Patient demographics.

	average (minimum ~ maximum)
Age	50.8 (36 ~ 62)
Age of onset	47 (37 ~ 56)
CAG Repeats	43 (41 ~ 46)
UHDRS TMS	27 (0 – 67)
UHDRS Behavior	11 (0 – 36)
UHDRS TFC	10 (2 – 14)
Stroop Color Word	34 (0 – 63)

2.3. Statistical methods

We conducted a statistical analysis to determine the correlation of the UHDRS scores with quantitative data of each region of interest obtained by differential tractography. Data was evaluated using a one-sided *t*-test and was then organized by longitudinal and cross-sectional analyses to determine the efficacy of the dynamic biomarker tested and have more control over brain regions tested and their correlation with clinical scores.

Longitudinal measures of subjects were modeled using the generalized estimating equation (GEE) model, a linear model similar to the mixed effect model that can investigate the correlation between tract volume and the clinical scores that evaluated the cognitive levels and severity of the disease. Sandwich estimate of the variance was used to avoid violations of normality.

Using the GEE model, we correlated differential tractography findings and UHDRS total scores for motor, cognitive, behavior, and functional capacity. Since the motor scores include assessments to evaluate the motor dysfunction in detail, we further correlated differential tractography with subscores under the motor assessment, including Total Motor Score (TMS), Dystonia Total, Chorea Total and Rapid Alternating Movements (RAM), to see whether there are meaningful findings specific to these subscores. The same setting was applied to the cognitive component represented by the subscore Stroop Color-Word. Lastly, the UHDRS Behavioral Total, and TFC (Total Functional Capacity) scores were correlated. Using our novel method, we obtained several tract bundles with decreased anisotropy. All bundles obtained by differential tractography were further segmented into five different white matter regions, which included cingulum, corpus callosum, corticostriatal pathway, corticospinal pathway, and the whole brain. This allowed us to study region-specific correlation.

Targeted fiber tracking analysis was performed for each scan using their corresponding differential tractography results. Quantitative data such as tract volume for each segmented region was registered as a reference for tract involvement, higher volumes indicate greater magnitude of affected tracts.

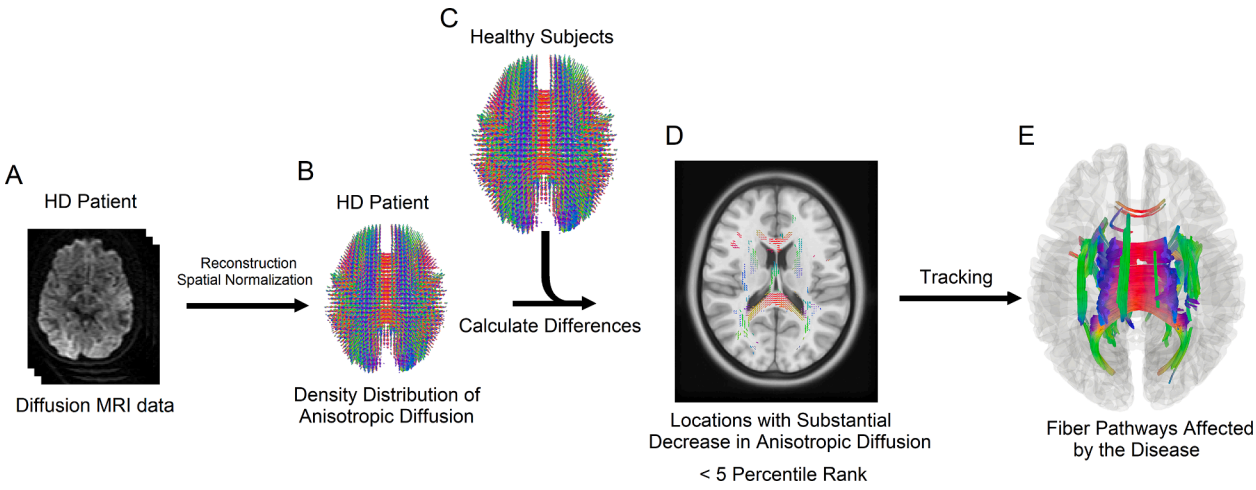

Fig. 1. Flowchart of the differential tractography analysis. The red–greenblue colors represents the orientation of diffusion (red: left–right, green: anterior-posterior, blue: superior-inferior). (A) The diffusion data of each subject was reconstructed in a common stereotaxic space using q-space diffeomorphic reconstruction (QSDR) to calculate the diffusible spin distribution function. (B) The reconstruction allows the visualization of the density distribution of the anisotropic diffusion of the subject in the standard space. (C) Values from a normal population are compared to the study subject to calculate the percentile rank. (D) Comparison is then used to map locations with anisotropic diffusion of subject sufficiently smaller than normal population (<5 percentile rank). (E) Fiber tracking algorithm is then associated with the data obtained by substantial decrease in anisotropic diffusion to map exact fiber pathways affected by the disease.

Overall, a total of 35 comparisons were performed to determine statistical correlation, which translate to 35 hypotheses, one for each longitudinal and cross-sectional analyses. For cross-sectional analysis, we correlated the volume extracted from each fiber bundle with each clinical score. Furthermore, we correlated the change in tract volume with the change in clinical scores which yielded 35 hypotheses. Each hypothesis was tested in repeat scans of pre-manifest and manifest subjects using the GEE model. We also studied these 35 correlation hypotheses for each scan time point (scans 1, 2, and 3) as three independent cross-sectional studies using the Spearman correlation model, a nonparametric method to investigate the correlation using the rank of the tract values.

The longitudinal change in tract volume and the clinical scores of the above-mentioned 35 correlation hypotheses, were also studied using the GEE model for the manifest patients. Three separate Spearman correlation analyses were conducted to study the change between scan one and scan two, scan one and scan three, and scan two and scan three. The hypothesis was tested using a one-sided tail *t*-test. A p-value of 0.05 was corrected using Bonferroni correction to obtain familywise significance and eliminate false positive results, yielding a *p-value* of 0.001 or less to be considered statistically significant. All analyses were conducted in SAS 9.3.

The statistics of this study and its interpretation were supervised by a statistician (YF. C.).

3. Results

3.1. Individual differential tractography results

Table 2 shows differential tractography volume measurements of cingulum, corpus callosum, corticostriatal pathway, corticospinal pathway, and whole brain in all manifest and premanifest subjects, which were mapped automatically by differential tractography. As noted in Table 2, increased tract volumes (mm3) denote reduced tract integrity compared to normal population. The color red in Table 2 helps to differentiate tracts with higher volume (dark red color) from tracts with lower volumes (light red color). The UHDRS Total Motor Score (TMS) and differential tractography results were assessed independently. Differential tractography progression was demonstrated in nine out of twelve manifest subjects (75%), and in one out of four premanifest subject (25%) with a time-dependent increased volume of affected tracts. Subjects A, B, and C were selected to demonstrate a correlation based on their UHDRS TMS, in which higher deteriorating motor function was evident (Fig. 2). Higher UHDRS TMS indicates worse performance, and all three subjects demonstrated an increased volume of affected tracts, likely correlating with decreased connectivity (Fig. 2). This progression corresponded with UHDRS TMS higher scores at each measurement, with the exception of subject C, in which an increase in the volume of degenerating tracts did not correspond with UHDRS TMS, remaining unchanged at 6-months compared to the baseline scan. To visualize inter-individual variability, please refer to Table S1.

3.2. Manifest versus premanifest patients

Significant differences were observed in the manifest and premanifest group. Initial scans in symptomatic patients demonstrated a significant number of affected bundles. In contrast none or a small number of affected tracts in the premanifest group (Table S1). These results provide further validation of this technique in identifying affected pathways and distinguishing presymptomatic from symptomatic patients.

3.3. Longitudinal versus cross-sectional analyses

Longitudinal data was evaluated to determine the correlation between affected tract volumes and UHDRS clinical scores. We performed two longitudinal analyses and the time frame was 6–12 months. First, we studied the correlation between UHDRS clinical scores and tract volumes in each brain region (cingulum, corpus callosum, corticostriatal pathway, corticospinal pathway, and whole brain). In addition, a second longitudinal analysis was performed to examine the correlation between change in clinical scores and the change in volumes of tracts, including cingulum, corpus callosum, corticostriatal pathway, corticospinal pathway, and whole brain.

Out of 35 correlations in our initial longitudinal analysis, twelve (34.3%) showed statistical significance between tract volume and clinical scores, which included 2 correlations (5.7%) with statistical significance ($p\text{-value} < 0.001$) and ten correlations (28.6%) statistically significant ($p\text{-value} < 0.0001$). In addition, all brain bundles (cingulum, corpus callosum, corticostriatal pathway, corticospinal pathway, and whole brain) significantly correlated with clinical scores as follows. UHDRS TMS was statistically significant ($p\text{-value} < 0.0001$) in cingulum

Table 2
Tract volume measurements in HD subjects.[a]

Subject	Scan	Manifest/ Premanifest	Cingulum Volume (mm^3)	Corpus Callosum Volume (mm^3)	Corticostriatal Pathway Volume (mm^3)	Corticospinal Pathway Volume (mm^3)	Whole Brain Volume (mm^3)
A	1	Manifest	760	6032	4736	2224	15103
	2		824	5360	5432	2040	17878
	3		1176	21152	8176	17112	39588
B	1	Manifest	1872	13336	0	19816	33236
	2		4120	35296	6352	21992	61214
	3		2656	26688	3096	26096	51240
C	1	Manifest	952	5248	968	15944	16502
	2		1312	21168	3624	37496	56512
	3		2096	23304	6440	39296	64686
D	1	Manifest	0	0	0	0	5917
	2		0	0	520	0	6323
	3		0	3184	752	0	10370
E	1	Manifest	3080	40032	4832	36200	77794
	2		5768	41640	608	31272	80894
F	1	Manifest	408	5872	688	1512	11690
	2		0	0	1048	1176	6413
	3		0	0	1352	0	5664
G	1	Manifest	1608	41504	1896	43168	87789
H	1	Manifest	37064	37064	13280	44872	119938
I	1	Premanifest	280	9144	7336	36184	55752
	2		0	1216	0	0	3769
	3		0	1984	664	2680	6223
J	1	Manifest	0	19352	4176	1736	23829
	2		1232	52248	9672	42800	97512
	3		1856	35184	8168	16608	60167
K	1	Manifest	592	9904	1776	14976	27213
	2		2808	48720	3480	43592	91088
	3		2104	28136	7944	28216	58704
L	1	Premanifest	0	0	0	280	130
M	1	Premanifest	0	272	840	5480	9763
	2		0	0	0	0	0
	3		0	0	0	0	0
N	1	Premanifest	0	0	224	3328	5059
	2		0	0	0	1192	2961
	3		816	4864	3464	17336	22114
O	1	Manifest	496	32096	8696	26536	60015
	2		560	41472	12128	32992	67966
	3		2608	66248	22800	56328	137436
P	1	Manifest	592	712	1816	656	7210
	2		0	3976	3664	1464	10892
	3		2344	34240	7416	10920	51041

* Higher tract volumes (mm^3) denotes reduced tract integrity compared to normal populations (dark red).

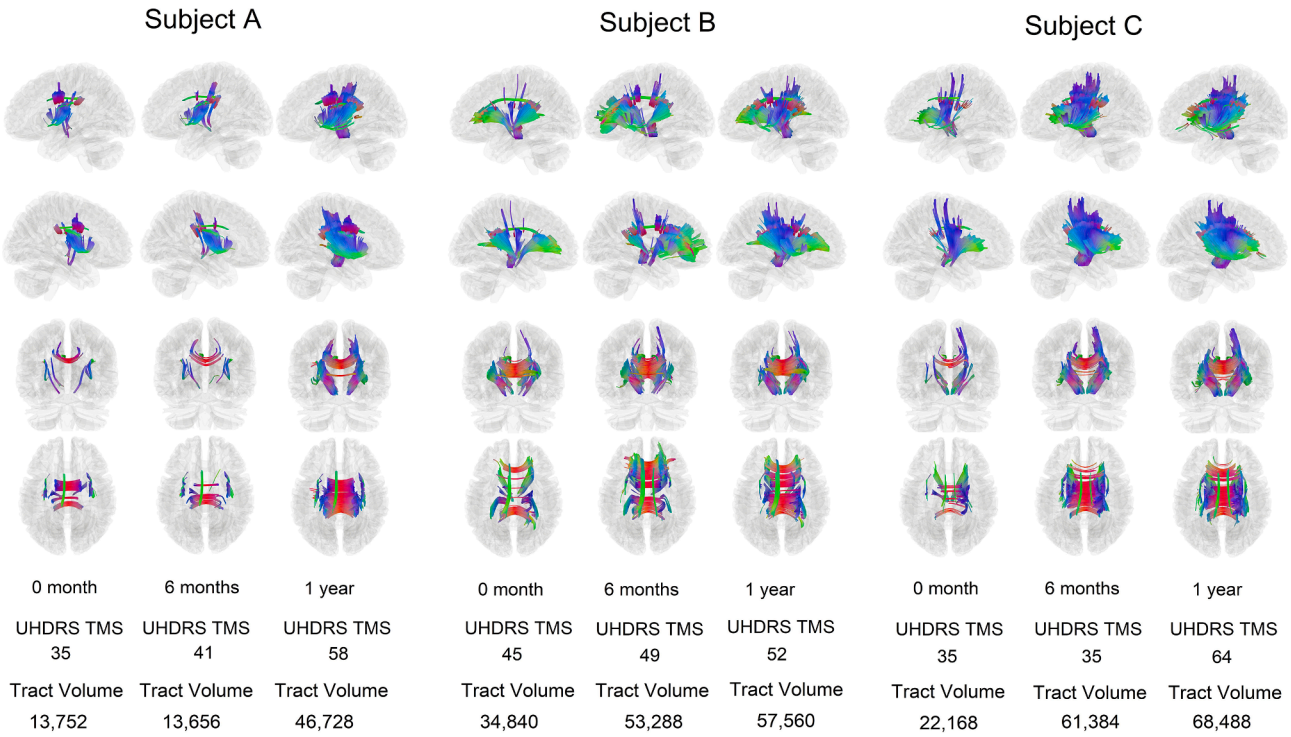

Fig. 2. Fiber pathways affected in three manifest subjects mapped by differential tractography. The red–greenblue colors represents the orientation of diffusion (red: left–right, green: anterior-posterior, blue: superior-inferior). Tract volumes are represented in mm^3. The greater the volume of affected fibers, the higher the UHDRS Total Motor Score (UHDRS TMS) that subjects will display, showing a deteriorating performance in motor functions. Subject A displays a significant correlation between fiber pathways affected and UHDRS TMS (35, 41, and 58) with increasing tract volumes (13,753 mm^3, 13,656 mm^3, and 46,728 mm^3) in three different scanning time points respectively (0 month, 6 months, 1 year). Subject B shows a UHDRS TMS of 45, 49, and 52 with tract volumes of 34,840 mm^3, 53,288 mm^3, and 57,560 mm^3 at 0 month, 6 months, and 1 year, respectively. Subject C is the subject with the most change among the three, with a UHDRS TMS of 35, 35, and 64 and tract volumes of 22,168 mm^3, 61,384 mm^3, and 68,488 mm^3 at 0 month, 6 months, and 1 year, respectively. Interestingly, subject C shows no change in the UHDRS TMS between 0 and 6 months, nevertheless, a significant increase in tract volume was observed in this time period (22,168 mm^3 and 61,384 mm^3 respectively), providing evidence that differential tractography can be used as a dynamic biomarker to predict pre-clinical manifestations.

and corticostriatal pathway; RAM was significant with cingulum, corpus callosum, corticostriatal and corticospinal pathway (*p-value* < 0.0001), and with whole brain (*p-value* < 0.0001); Stroop color-word was significant with Cingulum and Corpus Callosum (*p-value* < 0.0001); and UHDRS TFC was significant with cingulum and corticostriatal pathway (*p-value* < 0.0001), and with corticospinal pathway (*p-value* < 0.001) (Table 3). Supplementary Tables S2 and S3 represent visual components of Table 3 for better visualization.

In the second longitudinal analysis, seven correlations (20%) were statistically significant (*p-value* < 0.0001) as follows. A statistical significance was observed in dystonia total with cingulum and corpus callosum (*p-value* < 0.0001); and RAM showed significance in all brain regions (*p-value* < 0.0001). Results from this analysis supports differential tractography as a practical and accurate biomarker for evaluating changes in volume of different brain regions in relation to clinical scores (Table 3).

Table 4 show results for cross-sectional and longitudinal data in manifest patients. Correlation analysis was applied to evaluate the relationship between clinical scores and tract volumes in cross-sectional data from the first, second, and third scans, yielding a total of 105 correlations that were corrected using Bonferroni correction to consider familywise significance. In addition, Table 5 shows results of correlation analysis which was applied to evaluate the relationship between the changes in all clinical scores and the changes in tract volumes in three separate groups: (1) changes observed from first to second scan, (2) changes observed from the first to the third scan, and (3) changes observed from the second to the third scan. No statistical significance was observed when tract volumes were compared to clinical scores in cross-sectional data, or when tract volumes were compared to the changes in clinical scores in longitudinal data (Tables 4 and 5). However, it is unlikely to achieve significance when familywise *p-value* is considered (Bonferroni correction) due to the small number of subjects included in the analysis, and this does not diminish the important findings obtained in the longitudinal analysis (Table 3). For better visualization, supplementary Table S4 and S5 represent visual components of Table 4 and Table 5, respectively.

Since this study does not examine individual fiber tracts, but rather white matter bundles as a group, any findings are common between subjects in majority. In addition, since subject data was normalized to a common space, the overlapped findings were examined and groupwise statistical significance was common in the population.

4. Discussion

In this study we evaluated differential tractography as a clinical translational tool by conducting correlation analyses between white matter volumes measurements and clinical scores in manifest and premanifest HD patients. Overall results indicate that differential tractography appears to be a robust dynamic biomarker with high statistical significance in longitudinal data to determine changes in tract volumes of white matter tracts with the potential to supplement the UHDRS in manifest and premanifest HD. Differential tractography appears to be a highly reliable monitoring biomarker to delimit changes exhibited in cingulum, corpus callosum, corticostriatal pathway, corticospinal pathway, and whole brain when correlated with UHDRS. Moreover, an increase of volume of damaged tracts was observed before symptom onset in one particular subject (Subject C, Fig. 2). This prediction power can be taken in consideration to anticipate onset at the premanifest stage

Table 3
Correlation analysis between tract volume and clinical scores in longitudinal data.

	Clinical scores	Correlation between clinical scores and tract volume			Correlation between the change in clinical scores and change in tract volumes		
		coefficient	*standard error*	*p-value*	*coefficient*	*standard error*	*p-value*
Cingulum	UHDRS TMS	0.088	0.018	**<.0001***	0.380	0.403	0.173
	Dystonia total	0.187	0.093	0.022	0.870	0.158	**<.0001***
	Chorea total	-0.032	0.118	0.608	-0.325	0.379	0.804
	RAM	0.522	0.075	**<.0001***	0.602	0.148	**<.0001***
	Stroop Color Word	-0.115	0.029	**<.0001***	0.032	0.216	0.559
	UHDRS Behavior	0.081	0.055	0.067	0.317	0.132	0.008
	UHDRS TFC	0.046	0.007	**<.0001***	-0.258	0.144	0.964
Corpus Callosum	UHDRS TMS	0.073	0.027	0.003	0.292	0.531	0.291
	Dystonia total	0.259	0.089	0.002	1.170	0.267	**<.0001***
	Chorea total	-0.030	0.163	0.572	-0.980	0.455	0.984
	RAM	0.438	0.124	**<.0001***	2.746	0.251	**<.0001***
	Stroop Color Word	-0.134	0.039	**<.0001***	0.538	1.069	0.693
	UHDRS Behavior	0.023	0.073	0.374	-0.045	0.208	0.586
	UHDRS TFC	0.033	0.013	0.005	-0.405	0.130	0.999
Corticostriatal Pathway	UHDRS TMS	0.070	0.013	**<.0001***	0.185	0.358	0.303
	Dystonia total	0.305	0.132	0.011	0.337	0.228	0.070
	Chorea total	0.058	0.097	0.276	-0.663	0.369	0.964
	RAM	0.420	0.073	**<.0001***	2.587	0.279	**<.0001***
	Stroop Color Word	-0.080	0.028	0.003	0.569	0.982	0.719
	UHDRS Behavior	-0.014	0.063	0.587	-0.121	0.181	0.748
	UHDRS TFC	0.030	0.007	**<.0001***	-0.071	0.074	0.831
Corticospinal Pathway	UHDRS TMS	0.054	0.025	0.015	0.288	0.396	0.234
	Dystonia total	0.169	0.161	0.147	0.458	0.278	0.050
	Chorea total	-0.069	0.143	0.685	-0.517	0.425	0.888
	RAM	0.408	0.097	**<.0001***	3.009	0.310	**<.0001***
	Stroop Color Word	-0.105	0.044	0.009	0.814	1.130	0.764
	UHDRS Behavior	0.028	0.069	0.344	-0.131	0.217	0.728
	UHDRS TFC	0.030	0.010	**0.001***	-0.171	0.087	0.976
Whole Brain	UHDRS TMS	0.053	0.020	0.003	0.385	0.446	0.194
	Dystonia total	0.145	0.058	0.006	0.560	0.301	0.031
	Chorea total	0.083	0.072	0.123	-0.548	0.441	0.893
	RAM	0.293	0.097	**0.001***	3.249	0.309	**<.0001***
	Stroop Color Word	-0.067	0.026	0.005	0.854	1.200	0.762
	UHDRS Behavior	-0.011	0.039	0.611	-0.094	0.225	0.661
	UHDRS TFC	0.021	0.007	0.002	-0.206	0.101	0.980

Significant (*p-value* <0.001).

*Familywise significant (*p-value* <0.05/35=0.001).

UHDRS: Unified Huntington Disease Rating Scale. TMS: Total motor score. RAM: Rapid alternating movements. TFC: Total functional capacity.

Table 4
Cross-sectional correlation between clinical scores and tract volume.

		First Scan		Second Scan		Third Scan	
	Clinical scores	*corr*	*p-value*	*corr*	*p-value*	*corr*	*p-value*
Cingulum	UHDRS TMS	0.345	0.136	0.735	0.012	-0.042	0.543
	Dystonia total	-0.114	0.638	0.138	0.362	-0.269	0.758
	Chorea total	-0.117	0.641	0.211	0.293	-0.517	0.923
	RAM	-0.025	0.531	0.397	0.145	0.209	0.294
	Stroop C W	-0.500†	0.049	-0.046	0.453	-0.343	0.183
	UHDRS Behavior	0.004	0.496	0.312	0.207	-0.025	0.526
	UHDRS TFC	0.240	0.226	0.594	0.046	0.176	0.326
Corpus Callosum	UHDRS TMS	-0.223	0.757	0.240	0.267	-0.417	0.868
	Dystonia total	-0.253	0.786	0.160	0.340	-0.698	0.982
	Chorea total	-0.246	0.780	0.101	0.398	-0.343	0.817
	RAM	-0.495	0.949	-0.034	0.534	-0.119	0.620
	Stroop C W	-0.347	0.135	0.315	0.796	-0.150	0.350
	UHDRS Behavior	0.239	0.227	0.228	0.278	0.285	0.229
	UHDRS TFC	-0.012	0.515	0.042	0.457	-0.433	0.878
Corticostriatal Pathway	UHDRS TMS	-0.050	0.561	-0.184	0.682	-0.033	0.534
	Dystonia total	0.027	0.467	-0.023	0.523	-0.213	0.709
	Chorea total	-0.042	0.552	-0.563	0.943	-0.251	0.743
	RAM	-0.412	0.909	0.042	0.457	0.111	0.388
	Stroop C W	0.028	0.535	-0.268	0.243	-0.133	0.366
	UHDRS Behavior	0.177	0.291	0.277	0.235	0.720	0.014
	UHDRS TFC	-0.071	0.586	-0.150	0.650	-0.100	0.601
Corticospinal Pathway	UHDRS TMS	0.110	0.367	0.251	0.257	0.460	0.106
	Dystonia total	-0.312	0.839	0.274	0.238	0.098	0.401
	Chorea total	0.032	0.461	0.345	0.182	0.046	0.453
	RAM	-0.279	0.810	-0.193	0.691	0.303	0.214
	Stroop C W	-0.305	0.168	0.351	0.823	-0.243	0.265
	UHDRS Behavior	0.165	0.304	-0.101	0.602	0.193	0.309
	UHDRS TFC	0.090	0.391	-0.133	0.634	0.243	0.265
Whole Brain	UHDRS TMS	0.046	0.444	0.251	0.257	0.067	0.432
	Dystonia total	-0.382	0.890	0.160	0.341	-0.289	0.775
	Chorea total	0.011	0.487	0.109	0.390	0.075	0.424
	RAM	-0.348	0.867	-0.025	0.526	-0.017	0.517
	Stroop C W	-0.273	0.196	0.268	0.757	-0.150	0.350
	UHDRS Behavior	0.147	0.324	0.252	0.256	0.167	0.333
	UHDRS TFC	0.067	0.418	0.067	0.432	-0.200	0.697

Positive Correlation.

Negative Correlation.

Familywise significant (*p-value* <0.05/35=0.001).

† Higher Stroop Color Word Score indicate better cognitive performance. Negative value does not indicate negative correlation.

UHDRS: Unified Huntington Disease Rating Scale. TMS: Total motor score. RAM: Rapid alternating movements. TFC: Total functional capacity.

Table 5
Cross-sectional correlation between change in clinical scores and the change in tract volumes.

		Change 1st scan to 2nd scan		Change: 1st to 3rd scan		Change: 2nd to 3rd scan	
	Clinical scores	*corr*	*p-value*	*corr*	*p-value*	*corr*	*p-value*
Cingulum	UHDRS TMS	0.477	0.097	-0.214	0.695	0.548	0.080
	Dystonia total	0.602	0.043	-0.400	0.837	0.115	0.393
	Chorea total	0.128	0.371	-0.539	0.916	0.445	0.135
	RAM	0.375	0.160	0.528	0.089	0.358	0.192
	Stroop C W	0.513	0.921	-0.707†	0.025	0.283	0.752
	UHDRS Behavior	0.351	0.177	0.313	0.225	0.602	0.057
	UHDRS TFC	0.427	0.126	-0.238	0.715	0.645	0.042
Corpus Callosum	UHDRS TMS	-0.067	0.568	0.071	0.433	0.335	0.208
	Dystonia total	0.842	0.002	-0.170	0.656	0.374	0.181
	Chorea total	-0.213	0.709	-0.455	0.871	0.417	0.152
	RAM	-0.220	0.716	0.712	0.024	-0.410	0.843
	Stroop C W	0.234	0.728	-0.503	0.102	0.755	0.985
	UHDRS Behavior	0.367	0.166	0.386	0.173	0.096	0.411
	UHDRS TFC	-0.233	0.727	-0.190	0.674	0.084	0.422
Corticostriatal Pathway	UHDRS TMS	-0.400	0.857	0.071	0.433	0.036	0.466
	Dystonia total	0.337	0.188	-0.170	0.656	-0.181	0.666
	Chorea total	-0.741	0.989	-0.455	0.871	-0.012	0.512
	RAM	-0.254	0.745	0.712	0.024	0.133	0.377
	Stroop C W	0.025	0.526	-0.503	0.102	0.419	0.849
	UHDRS Behavior	0.183	0.318	0.386	0.173	0.431	0.143
	UHDRS TFC	-0.083	0.584	-0.190	0.674	0.503	0.102
Corticospinal Pathway	UHDRS TMS	-0.483	0.906	0.238	0.285	0.048	0.455
	Dystonia total	0.614	0.039	0.012	0.489	0.410	0.157
	Chorea total	-0.383	0.846	-0.491	0.892	-0.147	0.636
	RAM	-0.576	0.948	0.589	0.062	-0.711	0.976
	Stroop C W	-0.008	0.492	-0.132	0.378	0.539	0.916
	UHDRS Behavior	0.333	0.190	0.506	0.100	-0.156	0.644
	UHDRS TFC	-0.467	0.897	0.262	0.265	-0.156	0.644
Whole Brain	UHDRS TMS	-0.150	0.650	0.071	0.433	0.347	0.200
	Dystonia total	0.703	0.017	-0.158	0.645	0.434	0.141
	Chorea total	-0.179	0.677	-0.419	0.849	0.209	0.310
	RAM	-0.297	0.781	0.565	0.072	-0.374	0.819
	Stroop C W	0.310	0.791	-0.395	0.166	0.790	0.990
	UHDRS Behavior	0.483	0.094	0.422	0.149	0.096	0.411
	UHDRS TFC	-0.083	0.584	0.071	0.433	0.192	0.325

Positive Correlation.

Negative Correlation.

Familywise significant (*p-value* <0.05/35=0.001).

† Higher Stroop Color Word Score indicate better cognitive performance. Negative value does not indicate negative correlation.

UHDRS: Unified Huntington Disease Rating Scale. TMS: Total motor score. RAM: Rapid alternating movements. TFC: Total functional capacity.

to characterize disease progression, adding great value and high reliability to differential tractography as a predictive monitoring biomarker. The use of different scanners will have introduced a fixed bias in our correlation analysis, bringing the same intercept for our variable. Thus, the correlation coefficient will not have been affected, since the scanner difference is the same for all subjects, and our hypothesis would have remained the same.

It is also noteworthy the distinction that differential tractography provides when comparing manifest vs premanifest individuals, as affected tracts in manifest subjects displayed higher tract volumes as expected, in opposition to gene-positive individuals who yielded few or no tracts at all (as seen in Supplementary Table S1), supporting the accuracy of the technique. Since differential tractography findings are associated with damage appearing in pathway trajectories, the technique provides the amount of degeneration (in volume measurements) in addition to providing a better localization of disease. In this sense, we have been able to map segments of dysconnectivity in white matter areas to find the link between lesions and grey matter to better understand functional changes due to neuronal degeneration. Therefore, our diffusion-based analysis technique exhibits a significant novelty over conventional tractography by differentiating errors in local voxels versus true findings that spread along a fiber trajectory. This in turn, provides a biological advantage for not only localizing neurodegeneration with precision, but also for tracking the evolution of disease and treatment response, as suggested by a previous study (Yeh et al., 2019). By applying deterministic tractography, we have an advantage by the novelty of the technique which is capable of resolving crossing fibers. Deterministic tractography makes use of quantitative anisotropy (QA) which relies on generalized q-sampling imaging (GQI) to estimate the orientation of individual fibers (Yeh et al., 2010), and spin distribution function (SDF) to provide the amount or density of diffusing water in any direction within a single voxel (Yeh et al., 2016), therefore posing a great value over widely used diffusivity-based estimations such as FA. The use of differential tractography paired with a robust clinical evaluation at the pre-clinical stage in gene positive asymptomatic populations, can be of utmost clinical significance in routine clinical follow-up, and although our study provides a small number of subjects, we acknowledge that future studies are granted to obtain robust measures for when assessment of new treatment and therapies are required in clinical trials.

4.1. Implications of the clinical data

Longitudinal analysis demonstrated the highest statistical correlation with progression of clinical UHDRS scores in all brain regions (cingulum, corpus callosum, corticostriatal pathway, and corticospinal pathway), in relation to UHDRS TMS, Stroop Color-Word, UHDRS Total Functional Capacity (TFC), and especially in relation to Rapid Alternating Movements (RAM), which was statistically significant (p-value $<$ 0.0001) in all brain regions. Since Bonferroni correction was applied to consider familywise significance in multiple comparison analyses, results from the cross-sectional analysis did not yield significant findings. However, this does not hinder the potential of differential tractography as a tool to further understand the biological mechanism of white matter loss, and further studies with larger samples are required to determine a true significant value in cross-sectional data and larger group studies. Despite this limitation, results further confirm the role of white matter pathways involved in HD progression (Poudel et al., 2014; Rosas et al., 2010). Demonstrated changes on differential tractography in both premanifest and manifest HD, and particularly in the earlier stages, may be of value in future longitudinal and cross-sectional studies (Poudel et al., 2015). In premanifest HD where clinical markers of disease progression do not exist, differential tractography can be used as a non-invasive tool to dynamically monitor clinically asymptomatic disease progression. In manifest HD, the observed disease progression made by differential tractography can be used to supplement existing clinical markers of progression.

4.2. Speculative mechanisms

Degeneration in the association, commissural and projection fibers are implicated in the course of the disease and its clinical manifestations. Degeneration of corticospinal and corticostriatal pathways white matter tracts are linked to changes in motor functions behavior, executive function, movement, and the lack of integration of motor and cognitive function resulting in progression of UHDRS TMS, RAM, Stroop Color Word, UHDRS TFC. Thus, statistical correlation of Corticospinal and corticostriatal pathways with UHDRS TMS, RAM, and UHDRS TFC supports the relationship with motor dysfunction, and studies have supported these findings in manifest HD, and several important behavioral changes such as global apathy have been recently associated with degeneration of corticostriatal pathway (De Paepe et al., 2019; Phillips et al., 2015). Statistical correlation exhibited by the corticospinal tract in relation to UHDRS TMS, Stroop Color Word, TFC, and especially with RAM corroborates the critical relationship between corticospinal tract demyelination and motor symptoms at the premanifest and manifest stages which is associated with progression of UHDRS motor scores (Phillips et al., 2015). The highest correlation found with respect to RAM in longitudinal data studied by differential tractography, is validated by the motor involvement of the disease. Therefore, differential tractography represents a novel monitoring biomarker allowing detection of the exact anatomical location of degeneration and its subsequent correlation with loss of clinical function as measured by existing markers of progression.

4.3. Differential tractography in relation to premanifest and manifest disease and UHDRS scores

Despite the small number of patients, significant differences were observed between the premanifest and manifest HD. Relatively few areas were affected in premanifest patients in relation to patients in the manifest group (as in Supplementary Table S1), thereby lending further credibility to this imaging method. As expected, significant progression was observed at 6 and 12 months in manifest patients in relation to the baseline scan. The observed increase in volume of affected tracts corresponded with an increase in the UHDRS clinical scores. Despite being a reliable gold-standard to determine clinical progression in HD for many years (Kieburtz et al., 2001), the UHDRS assessment can be prone to variability. Differential tractography as an automated method is less prone to variability, and can supplement the use of the UHDRS in manifest HD. In premanifest patients, differential tractography can demonstrate changes in white matter preceding disease onset.

4.4. Future directions and limitations

We demonstrate the feasibility of differential tractography as a potential biomarker to anticipate disease onset in premanifest and manifest HD. Our main limitation was the small number of subjects which prevented obtaining statistical significance in cross-sectional data, and this limitation prevented us to obtain a more homogeneous clinical and longitudinal data. Additional research with larger samples is required to obtain a clear validation. We acknowledge that we cannot estimate effect size, as the method is for individual diagnosis which places more emphasis on sensitivity and specificity. Therefore, although differential tractography has potential for group diagnosis, future studies with a greater number of subjects will be necessary to evaluate the effect size at the group level. We did not account for time between scans in the statistical model, and this will certainly be a variable which must be considered in future larger studies. In addition, premanifest HD diagnosis was made based of genetic profile and we did not acquire clinical markers such as CAP score (CAG - Age Product Scaled score) or DBS (Disease Burden Score), for which we will consider obtaining in future

studies. There is a mismatch between differential tractography and the UHDRS TMS in few cases as shown by one patient (subject F, Table S1) with decreasing volumes and progression of the UHDRS TMS. In manifest HD, differential tractography demonstrated changes or progression at an anatomical level that may not be readily discernible with UHDRS scores. At this stage we do not have a clear understanding of the nature of the mismatch and thus differential tractography will require further validation in a larger study. Lastly, although differential tractography provides encouraging results to carry future larger studies, we recognize the limitation that differences between manifest and premanifest patients cannot be generalizable due to the small number of subjects in each group. Nevertheless, the overall findings confirmed the applicability of differential tractography as a dynamic non-invasive biomarker. Differential tractography can be considered in future studies with larger cohorts with more homogenous clinical and longitudinal data to assess the efficacy of therapeutic trials particularly in premanifest HD, where future drug trials will be aimed to prevent symptomatic conversion.

Data availability statement

Data supporting the findings of this study are not publicly available as it contains sensitive information that may compromise the privacy of the participants of this study.

CRediT authorship contribution statement

Jessica V. Barrios-Martinez: Investigation, Writing – original draft, Writing – review & editing, Visualization. **David T. Fernandes-Cabral:** Formal analysis, Investigation, Writing – original draft. **Kumar Abhinav:** Writing – review & editing. **Juan C. Fernandez-Miranda:** Funding acquisition, Conceptualization, Supervision. **Yue-Fang Chang:** Formal analysis, Validation, Supervision. **Valerie Suski:** Data curation, Investigation, Supervision, Validation, Writing – review & editing. **Fang-Cheng Yeh:** Data curation, Funding acquisition, Methodology, Project administration, Software, Supervision, Writing – review & editing, Visualization. **Robert M. Friedlander:** Conceptualization, Funding acquisition, Investigation, Supervision, Writing – review & editing.

Declaration of Competing Interest

The authors declare the following financial interests/personal relationships which may be considered as potential competing interests: Dr. Robert M. Friedlander is on the Board of NeuBase Therapeutics and Difusion Technologies. All other authors report no conflict of interest.

Acknowledgment

We dedicate this work to the memory of Milton Fine whose foundation provided initial funding for this work. This study was partly supported by NIMH of the National Institutes of Health, United States under award number R56MH113634. The development of the analytical approach was partly supported by NIDCD of the National Institutes of Health, United States under award number R01DC013803. Additional support came from Walter L. Copeland Fund of the Pittsburgh Foundation, United States. The content is solely the responsibility of the authors and does not necessarily represent the official views of the National Institutes of Health.

Appendix A. Supplementary data

Supplementary data to this article can be found online at https://doi.org/10.1016/j.nicl.2022.103062.

References

Adanyeguh, I.M., Branzoli, F., Delorme, C., Méneret, A., Monin, M.-L., Luton, M.-P., Durr, A., Sabidussi, E., Mochel, F., 2021. Multiparametric characterization of white matter alterations in early stage Huntington disease. Sci. Rep. 11 (1).

Basser, P.J., Mattiello, J., LeBihan, D., 1994. MR diffusion tensor spectroscopy and imaging. Biophys. J. 66 (1), 259–267.

Berlot, R., Metzler-Baddeley, C., Jones, D.K., O'Sullivan, M.J., 2014. CSF contamination contributes to apparent microstructural alterations in mild cognitive impairment. Neuroimage 92, 27–35.

Beukema, P., Yeh, F.C., Verstynen, T., 2015. In vivo characterization of the connectivity and subcomponents of the human globus pallidus. Neuroimage. 120, 382–393.

Biglan, K.M., Ross, C.A., Langbehn, D.R., Aylward, E.H., Stout, J.C., Queller, S., Carlozzi, N.E., Duff, K., Beglinger, L.J., Paulsen, J.S., 2009. Motor abnormalities in premanifest persons with Huntington's disease: the PREDICT-HD study. Mov. Disord. 24 (12), 1763–1772.

Craufurd, D., Thompson, J.C., Snowden, J.S., 2001. Behavioral changes in Huntington disease. Cogn. Behav. Neurol. 14, 219–226.

De Paepe, A.E., Sierpowska, J., Garcia-Gorro, C., Martinez-Horta, S., Perez-Perez, J., Kulisevsky, J., Rodriguez-Dechicha, N., Vaquer, I., Subira, S., Calopa, M., Muñoz, E., Santacruz, P., Ruiz-Idiago, J., Mareca, C., de Diego-Balaguer, R., Camara, E., 2019. White matter cortico-striatal tracts predict apathy subtypes in Huntington's disease. NeuroImage: Clinical. 24, 101965.

Donos, C., Mălîia, M.D., Mîndruță, I., Popa, I., Ene, M., Bălănescu, B., Ciurea, A., Barborica, A., 2016. A connectomics approach combining structural and effective connectivity assessed by intracranial electrical stimulation. Neuroimage. 132, 344–358.

Dumas, E.M., van den Bogaard, S.J.A., Ruber, M.E., Reilmann, R., Stout, J.C., Craufurd, D., Hicks, S.L., Kennard, C., Tabrizi, S.J., van Buchem, M.A., van der Grond, J., Roos, R.A.C., 2012. Early changes in white matter pathways of the sensorimotor cortex in premanifest Huntington's disease. Hum. Brain Mapp. 33 (1), 203–212.

Farquharson, S., Tournier, J.-D., Calamante, F., Fabinyi, G., Schneider-Kolsky, M., Jackson, G.D., Connelly, A., 2013. White matter fiber tractography: why we need to move beyond DTI. J. Neurosurg. 118 (6), 1367–1377.

Fernandez-Miranda, J.C., 2013. Beyond diffusion tensor imaging. J. Neurosurg. 118, 1363–1366.

Georgiou-Karistianis, Nellie, et al., 2011. Diffusion tensor imaging in Huntington's disease reveals distinct patterns of white matter degeneration associated with motor and cognitive deficits. Brain Imaging Behav. https://doi.org/10.1007/s11682-011-9121-8.

Gregory, S., Cole, J.H., Farmer, R.E., Rees, E.M., Roos, R.A.C., Sprengelmeyer, R., Durr, A., Landwehrmeyer, B., Zhang, H., Scahill, R.I., Tabrizi, S.J., Frost, C., Hobbs, N.Z., 2015. Longitudinal diffusion tensor imaging shows progressive changes in white matter in Huntington's disease. J. Huntington's Dis. 4 (4), 333–346.

Henf, J., Grothe, M.J., Brueggen, K., Teipel, S., Dyrba, M., 2018. Mean diffusivity in cortical gray matter in Alzheimer's disease: The importance of partial volume correction. NeuroImage: Clinical. 17, 579–586.

Hula, W.D., Panesar, S., Gravier, M.L., Yeh, F.-C., Dresang, H.C., Dickey, M.W., Fernandez-Miranda, J.C., 2020. Structural white matter connectometry of word production in aphasia: an observational study. Brain. 143 (8), 2532–2544.

Jeurissen, B., Leemans, A., Tournier, J.-D., Jones, D.K., Sijbers, J., 2013. Investigating the prevalence of complex fiber configurations in white matter tissue with diffusion magnetic resonance imaging. Hum. Brain Mapp. 34 (11), 2747–2766.

Kieburtz, K., et al., 2001. Unified Huntington's disease rating scale: reliability and consistency. Neurology. 11, 136–142.

Klöppel, S., Draganski, B., Golding, C.V., Chu, C., Nagy, Z., Cook, P.A., Hicks, S.L., Kennard, C., Alexander, D.C., Parker, G.J.M., Tabrizi, S.J., Frackowiak, R.S.J., 2008. White matter connections reflect changes in voluntary-guided saccades in pre-symptomatic Huntington's disease. Brain. 131 (1), 196–204.

Macdonald, V., Halliday, G., 2002. Pyramidal cell loss in motor cortices in Huntington's disease. Neurobiol. Dis. 10 (3), 378–386.

Melonakos, E.D., Shenton, M.E., Rathi, Y., Terry, D.P., Bouix, S., Kubicki, M., 2011. Voxel-based morphometry (VBM) studies in schizophrenia—can white matter changes be reliably detected with VBM? Psychiatry Res. Neuroimaging. 193 (2), 65–70.

Metzler-Baddeley, C., O'Sullivan, M.J., Bells, S., Pasternak, O., Jones, D.K., 2012. How and how not to correct for CSF-contamination in diffusion MRI. Neuroimage. 59 (2), 1394–1403.

Müller, H.-P., Grön, G., Sprengelmeyer, R., Kassubek, J., Ludolph, A.C., Hobbs, N., Cole, J., Roos, R.A.C., Duerr, A., Tabrizi, S.J., Landwehrmeyer, G.B., Süssmuth, S.D., 2013. Evaluating multicenter DTI data in Huntington's disease on site specific effects: An ex post facto approach. NeuroImage: Clinical. 2, 161–167.

Müller, H.-P., Gorges, M., Grön, G., Kassubek, J., Landwehrmeyer, G.B., Süßmuth, S.D., Wolf, R.C., Orth, M., 2016. Motor network structure and function are associated with motor performance in Huntington's disease. J. Neurol. 263 (3), 539–549.

Nopoulos, P.C., Aylward, E.H., Ross, C.A., Johnson, H.J., Magnotta, V.A., Juhl, A.R., Pierson, R.K., Mills, J., Langbehn, D.R., Paulsen, J.S., 2010. Cerebral cortex structure in prodromal Huntington disease. Neurobiol. Dis. 40 (3), 544–554.

Oh, S.L., Chen, C.-M., Wu, Y.-R., Valdes Hernandez, M., Tsai, C.-C., Cheng, J.-S., Chen, Y.-L., Wu, Y.-M., Lin, Y.-C., Wang, J.-J., 2013. Fixel-Based Analysis Effectively Identifies White Matter Tract Degeneration in Huntington's Disease. Front. Neurosci. 15, 1191.

Parker, G.D., Marshall, D., Rosin, P.L., Drage, N., Richmond, S., Jones, D.K., 2013. A pitfall in the reconstruction of fibre ODFs using spherical deconvolution of diffusion MRI data. Neuroimage. 65, 433–448.

Phillips, O., Sanchez-Castaneda, C., Elifani, F., Maglione, V., Di Pardo, A., Caltagirone, C., Squitieri, F., Sabatini, U., Di Paola, M., Tang, Y.-P., 2013. Tractography of the corpus callosum in Huntington's disease. PLoS ONE 8 (9), e73280.

Phillips, O., Squitieri, F., Sanchez-Castaneda, C., Elifani, F., Griguoli, A., Maglione, V., Caltagirone, C., Sabatini, U., Di Paola, M., 2015. The corticospinal tract in Huntington's disease. Cereb. Cortex 25 (9), 2670–2682.

Poudel, G.R., Stout, J.C., Domínguez D, J.F., Salmon, L., Churchyard, A., Chua, P., Georgiou-Karistianis, N., Egan, G.F., 2014. White matter connectivity reflects clinical and cognitive status in Huntington's disease. Neurobiol. Dis. 65, 180–187.

Poudel, G.R., Stout, J.C., Domínguez D., J.F., Churchyard, A., Chua, P., Egan, G.F., Georgiou-Karistianis, N., 2015. Longitudinal change in white matter microstructure in Huntington's disease: the IMAGE-HD study. Neurobiol. Dis. 74, 406–412.

Rosas, H.D., Lee, S.Y., Bender, A.C., Zaleta, A.K., Vangel, M., Yu, P., Fischl, B., Pappu, V., Onorato, C., Cha, J.-H., Salat, D.H., Hersch, S.M., 2010. Altered white matter microstructure in the corpus callosum in Huntington's disease: implications for cortical "disconnection". Neuroimage. 49 (4), 2995–3004.

Ross, C.A., Aylward, E.H., Wild, E.J., Langbehn, D.R., Long, J.D., Warner, J.H., Scahill, R. I., Leavitt, B.R., Stout, J.C., Paulsen, J.S., Reilmann, R., Unschuld, P.G., Wexler, A., Margolis, R.L., Tabrizi, S.J., 2014. Huntington disease: natural history, biomarkers and prospects for therapeutics. Nat. Rev. Neurol. 10 (4), 204–216.

Sotiropoulos, S.N., Jbabdi, S., Xu, J., Andersson, J.L., Moeller, S., Auerbach, E.J., Glasser, M.F., Hernandez, M., Sapiro, G., Jenkinson, M., Feinberg, D.A., Yacoub, E., Lenglet, C., Van Essen, D.C., Ugurbil, K., Behrens, T.E.J., 2013. Advances in diffusion MRI acquisition and processing in the Human Connectome Project. Neuroimage. 80, 125–143.

Tabrizi, S.J., Langbehn, D.R., Leavitt, B.R., Roos, R.AC., Durr, A., Craufurd, D., Kennard, C., Hicks, S.L., Fox, N.C., Scahill, R.I., Borowsky, B., Tobin, A.J., Rosas, H. D., Johnson, H., Reilmann, R., Landwehrmeyer, B., Stout, J.C., 2009. Biological and clinical manifestations of Huntington's disease in the longitudinal TRACK-HD study: cross-sectional analysis of baseline data. The Lancet Neurology. 8 (9), 791–801.

Tan, B., Shishegar, R., Poudel, G.R., Fornito, A., Georgiou-Karistianis, N., 2021. Cortical morphometry and neural dysfunction in Huntington's disease: A review. Eur. J. Neurol. 28 (4), 1406–1419.

Thu, D.C.V., Oorschot, D.E., Tippett, L.J., Nana, A.L., Hogg, V.M., Synek, B.J., Luthi-Carter, R., Waldvogel, H.J., Faull, R.L.M., 2010. Cell loss in the motor and cingulate cortex correlates with symptomatology in Huntington's disease. Brain. 133 (4), 1094–1110.

Tournier, J.-D., Calamante, F., Gadian, D.G., Connelly, A., 2004. Direct estimation of the fiber orientation density function from diffusion-weighted MRI data using spherical deconvolution. Neuroimage. 23 (3), 1176–1185.

Tournier, J.-D., Mori, S., Leemans, A., 2011. Diffusion tensor imaging and beyond. Magn Reson Med. 65 (6), 1532–1556.

Tuch, D.S., Reese, T.G., Wiegell, M.R., Van J. Wedeen, 2003. Diffusion MRI of complex neural architecture. Neuron 40 (5), 885–895.

Wang, Y., Wang, Q., Haldar, J.P., Yeh, F.-C., Xie, M., Sun, P., Tu, T.-W., Trinkaus, K., Klein, R.S., Cross, A.H., Song, S.-K., 2011. Quantification of increased cellularity during inflammatory demyelination. Brain. 134 (12), 3590–3601.

Weaver, K.E., Richards, T.L., Liang, O., Laurino, M.Y., Samii, A., Aylward, E.H., 2009. Longitudinal diffusion tensor imaging in Huntington's Disease. Exp. Neurol. 216 (2), 525–529.

Yeh, F.-C., Vettel, J.M., Singh, A., Poczos, B., Grafton, S.T., Erickson, K.I., Tseng, W.-Y., Verstynen, T.D., Diedrichsen, J., 2016. Quantifying differences and similarities in whole-brain white matter architecture using local connectome fingerprints. PLoS Comput. Biol. 12 (11), e1005203.

Yeh, F.-C., Panesar, S., Fernandes, D., Meola, A., Yoshino, M., Fernandez-Miranda, J.C., Vettel, J.M., Verstynen, T., 2018. Population-averaged atlas of the macroscale human structural connectome and its network topology. Neuroimage. 178, 57–68.

Yeh, F.C., Wedeen, V.J., Tseng, W.Y., 2010. Generalized q-sampling imaging. IEEE Trans Med Imaging. 29, 1626–1635.

Yeh, F.-C., Tseng, W.-Y., 2011. NTU-90: a high angular resolution brain atlas constructed by q-space diffeomorphic reconstruction. Neuroimage. 58 (1), 91–99.

Yeh, F.C., Tang, P.F., Tseng, W.Y., 2013a. Diffusion MRI connectometry automatically reveals affected fiber pathways in individuals with chronic stroke. Neuroimage Clin. 2, 912–921.

Yeh, F.-C., Verstynen, T.D., Wang, Y., Fernández-Miranda, J.C., Tseng, W.-Y., Zhan, W., 2013b. Deterministic diffusion fiber tracking improved by quantitative anisotropy. PLoS ONE 8 (11), e80713.

Yeh, F.-C., Zaydan, I.M., Suski, V.R., Lacomis, D., Richardson, R.M., Maroon, J.C., Barrios-Martinez, J., 2019. Differential tractography as a track-based biomarker for neuronal injury. Neuroimage. 202, 116131.

Zeun, P., McColgan, P., Dhollander, T., Gregory, S., Johnson, E.B., Papoutsi, M., Nair, A., Scahill, R.I., Rees, G., Tabrizi, S.J., 2022. Timing of selective basal ganglia white matter loss in premanifest Huntington's disease. NeuroImage: Clinical. 33, 102927.

Zhang, H., Wang, Y., Lu, T., Qiu, B.o., Tang, Y., Ou, S., Tie, X., Sun, C., Xu, K.e., Wang, Y., 2013. Differences between generalized q-sampling imaging and diffusion tensor imaging in the preoperative visualization of the nerve fiber tracts within peritumoral edema in brain. Neurosurgery. 73 (6), 1044–1053.